

Advances in Airborne Gravity and Magnetics

Fairhead, J.D.^[1,2], Cooper, G.R.J.^[3], Sander, S.^[4]

1. JD GeoConsultancy Ltd., Greystones, LS19 6QU, UK

2. School of Earth and Environment, University of Leeds, UK

3. School of Geosciences, University of the Witwatersrand, Johannesburg 2050, South Africa

4. Sander Geophysics

ABSTRACT

This contribution reviews the advances of gravity (including gradiometer) and magnetic methods of exploration during the last decade. The review is restricted to airborne methods of data acquisition since they are the most common method of acquisition. During this period gradiometer (FTG and AGG) methods have ‘come of age’ and both systems are providing gravity tensor data that image shallow targets as never before. This in part has been due to a significant reduction in instrument and processing noise levels. For gravity acquisition systems, their improvement in design and performance has led to better acquisition in turbulent air conditions. This now makes it possible to jointly conduct gravity and magnetic drape surveys. Improvements in processing and interpretation have gone hand in hand with improvements in acquisition. The greater use of the phase signal in the form of the tilt and local wavenumber derivatives in structural mapping, the benefits of finite depth estimation and a more stable downward continuation method are discussed.

INTRODUCTION

This decennial review (2007-2017) covers both airborne gravity gradiometer systems and airborne gravity and magnetic systems. Airborne gravity gradiometer systems, have ‘come of age’ during the last 10 years and have been proven to be an outstanding success in both mineral and oil-gas exploration by identifying and mapping gravity gradients associated with near surface mineral occurrences and shallow geological structures within ~2 km depth of the surface. Despite such success, the role of airborne gravity acquisition has not diminished but with its increased resolution in the presence of air turbulence, is now routinely combined with magnetic sensors on a single platform to provide an ideal drape survey choice for both regional and targeted resource evaluation studies in both the mineral and oil-gas sectors. During the last decade advances in all the above airborne instrumentation, data acquisition, processing and interpretation methodologies, and techniques have progressively reduced survey noise and increased overall survey resolution. This contribution reviews many of the advances over the last 10 years and in particular the instrumentation and the greater use of phase signal in advanced processing and interpretation.

The history of the use of gravity gradiometer and gravity and magnetic methods in resource exploration is more than adequately provided by the decennial review articles contained in the numerous volumes of Exploration, that have reported the proceedings of the International Conference on Mineral Exploration (Dransfield, 2007 and Thomson et al., 2007 in Exploration '07, and Reeves et al., 1997 in Exploration '97). The topic of gravity gradiometry is also contained in two papers of this volume (Hodges and Christensen, 2017; Smiarowski and Tianyou, 2017).

AIRBORNE GRAVITY GRADIOMETER SYSTEMS

This topic and its application to mineral and oil-gas targets has been extensively reported via a series of ASEG-PESA Airborne Gravity workshop papers in 2004 (Lane, 2004), 2010 (Lane, 2010) and 2016 (Lane, 2017). There are two commercial systems available, both built by Lockheed Martin, that provide high resolution gravity gradiometer data. These are *the Airborne Gravity Gradiometer* (AGG) developed in 1996 for BHP and known as the “Falcon” system with its first survey flown in 1999. The other gradiometer is *the Full Tensor Gradiometer* (FTG) originally operated as a marine instrument in 1994 but converted for airborne use in 2003. Gravity gradients (units of Eötvös, Eö) are measured directly within these instruments, where $1 \text{ Eö} = 10^{-9}/\text{s}^2 = 0.1 \text{ mGal}/\text{km}$. Three oil and mineral exploration contractors currently fly such equipment (CGG with Falcon-AGG, HeliFalcon and Falcon Plus; Bell Geospace with FTG; and AustinBridgeport with FTG). Airborne magnetic measurements are routinely acquired during gradiometer surveys. During the last decade the AGG and FTG systems together with aeromagnetic systems have been extensively and very successfully used in the oil and mineral industries for targeted resource evaluation studies.

Details of the gradiometer systems are:

Airborne Gravity Gradiometer (AGG): This instrument, also known as the Falcon, consists of a single spinning disk of diameter approximately 30 cm with eight equi-spaced accelerometers in a circle with their sensitive axes tangential to the circle. The accelerometers are linked into four opposing pairs, to measure differences in gravity response with two of the pairs measuring gravity differences in the opposite sense so that the system is immune to changes in rotation rate. The disk is

mounted on a high performance inertial stabilized platform, such that the disk spins in the horizontal plane i.e. the disk rotates about a near vertical axis. In this configuration it is able to provide lower-noise data, particularly in turbulence conditions, than systems with larger spin axis inclinations (Lee, 2001; Dransfield and Christensen, 2013).

Full Tensor Gradiometer (FTG): This instrument consists of twelve accelerometers with four accelerometers located on each of three slow spinning disks approximately 15 cm in diameter. The four accelerometers per disk are arranged in opposing pairs and each of the three disks has a spin axis arranged in mutually orthogonal directions (“umbrella” configuration) such that all three axes subtend an equal angle of 55° to the vertical. Each pair of accelerometers measures the difference in Earth’s gravity field such that the large dynamic accelerations experienced by the platform (i.e. aircraft) on which the instrument is located are cancelled out. Of the nine Tensor values (i.e. three Tensors or gradients for each of the three Cartesian gravity vectors), only five need to be measured since three pairs of Tensors are identical and T_{zz} Tensor can be derived directly from T_{xx} and T_{yy} using Laplace’s equation.

During the latter part of the decade significant instrument developments have and are being made to reduce volume and weight of the instrument and significantly increase sensitivity to reduce instrument noise.

These instruments include:

- **Falcon Plus:** Since 2005 the Falcon-AGG has been upgraded to a fully digital electronic system which has resulted in smaller and lighter gradiometers (Falcon Plus and HeliFalcon) allowing them to be installed on smaller aircraft, particularly helicopters. The Falcon Plus instrument has been in commercial use since 2012 and benefits from a number of significant improvements in data quality and efficiency (van Galder, 2017) that has halved the noise, decreased the instrument’s weight and size, and enhanced its processing to increase spatial resolution. When used alongside CGG’s strap-down gravity meter, sGrav, it is known as **Full Spectrum Falcon** which had its first commercial survey in 2016. The sGrav contains 3 component accelerometers and gyros and is designed to augment the long wavelength gravity signal that is less accurately measured by gravity gradiometers.
- **Full Spectrum Gravity (FSG):** Bell Geospace are reported (C. Murphy, pers. comm., 2017) to be offering this FSG as a standard deliverable. Back in the 1990s it was called T_{ze} , or Enhanced Gravity which consisted of combining FTG data to conventional gravity data measured by a Gravity Measuring Assembly (GMA) unit attached to the FTG instrument. Equally the GMA could be other terrestrial/satellite gravity anomaly data.
- **dFTG:** This is a digital FTG that will result in an estimated 30% reduction in volume and a 40% reduction in weight. This will allow it to be more easily installed in helicopters and other small aircraft (Meyer, 2017).
- **eFTG:** This is an enhanced FTG currently being developed under contract between AustinBridgeport and Lockheed Martin. It has increased sensitivity and signal to noise ratio by increasing the size of the spinning disks and doubling the number of accelerometers per disk (similar to the disk used in the AGG). This allows it to image smaller targets at greater depths as illustrated in Figure 1 for a cluster of kimberlite pipes. However, this all comes at the expense of increased weight and size of the carousel that could limit the size of aircraft it can be used in. It is scheduled to commence flight trials in mid-2017 with its first commercial survey hopefully before the end of 2017.
- **FTGplus:** Currently Lockheed Martin and CGG have a joint research project that is focused on using an architecture of non-rotating accelerometers which could provide 20 times the improvement over the current system (Meyer, 2017; Smiarowski and Tianyou, 2017) and mounted on a spherical air bearing-based platform that seeks to provide sub-Eö airborne performance.

Operationally the use of the gradiometer in the mineral and oil-gas industries has been highly dependent on the state of the commodity markets. Pre-2007 gradiometer applications were predominantly associated with mineral exploration, followed from 2009 to 2012 in a 50-50 split between minerals and oil-gas, and since 2012 with the downturn in the mineral sector has been predominantly oil-gas.

The performance of airborne gravity gradiometers (AGG and FTG) in terms of noise and sampling has been reported by Dransfield (2007), Dransfield and Christensen (2013) and van Galder (2016) and indicate that the vertical gravity gradient (G_{DD}) of AGG regularly achieved average survey noise levels of ~ 2 Eö. The noise reduction advantages of AGG is the size of its disk which gives it ~ 2.7 times lower noise than the FTG equivalent and that it mainly measures horizontal accelerations which are less sensitive to noise due to air turbulence. The advantage of the FTG having three spinning disks to AGG’s one is counter balanced by the inclined geometry of the FTG disks which can pick up noise from air turbulence which is non-linear (i.e. doubling air turbulence increases noise by more than a factor of 2) (Barnes and Lumley, 2010). Brewster (2016a; 2016b) and C. Murphy (pers. comm., 2017) however shows that although FTG raw data is inherently noisier, that after noise reduction processing T_{zz} noise levels can be as low as 1.44 - 2.0 Eö.

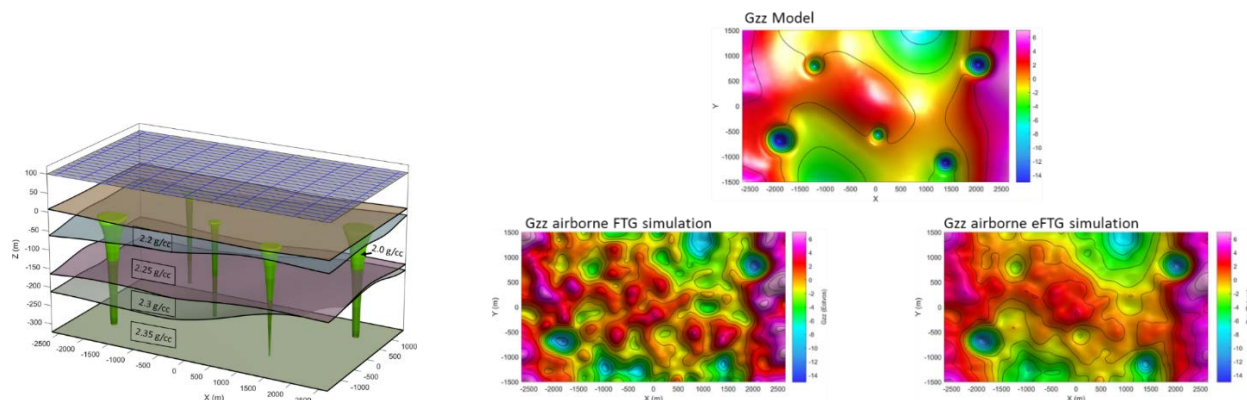


Figure 1: Simulation of FTG and eFTG data (right), based on a model containing a cluster of kimberlite pipes (shown in green) on the left. The eFTG kimberlite pipe anomalies are easier to identify from the background noise. The airborne survey simulation has line spacing of 100 x 500 m, flight height of 100 m above surface of model, air speed 64 m/s, measurement bandwidth of 0.2 Hz and assumed noise levels set at $10 E / \sqrt{Hz}$ for the FTG and $3.5 / \sqrt{Hz}$ for the eFTG (figure courtesy of AustinBridgeport).

Survey design and practice are as important as system noise since using Tensor data allows prediction of the field between survey lines and beyond survey edges (Brewster, 2011; Dransfield and Christensen, 2013; Barnes, 2014). This interpolation between lines allows the optimal resolution to target geology enabling target areas to be infilled in detail opposed to blind infill. Pilkington and Shamsipour (2014) have also shown that using the Kriging method of Tensor gridding can significantly reduce instrument and geological noise levels of a survey so that coherent geological meaningful anomaly patterns are better revealed.

The decade has shown an ever increasing resolution and accuracy of AGG and FTG gradiometer surveys resulting in a need to pay particular attention to measuring and removal of gravity gradient responses due to the 3D topographic relief and near surface 3D density variations, these being the closest mass targets to the instrument. If not removed they will represent geological noise in the data that can obscure geological signal of interest (Pilkington and Shamsipour, 2014). At greater depths, Stadtler et al (2014) have evaluated the resolution of T_z (gravity) and T_{zz} (vertical gravity gradient) verses depth to show that down to ~2 km depth the gradient methods provide more detail than conventional gravity surveys with the reverse happening progressively at greater depths. The success at shallow depths has been amply demonstrated in recent hydrocarbon exploration studies in Uganda by Tullow in 2009 (using FTG) and then by Total in 2010-2011 (using AGG, Price et al., 2013) and the spectacular successes by Tullow Oil in Kenya (using FTG) where the first eight gravity gradiometer highs they drilled were all petroleum systems. (see Bridgeport and Tullow Oil websites).

The vertical gradient Tensor, G_{DD} , (for AGG) or, T_{zz} , (for FTG) of the gravity field has been invariably used by contractors to image the gravity gradient response due to its amplitude sensitivity and symmetric response to underlying structures. The challenge over the decade, apart from noise reduction, has been to use all the Tensor components together in advanced processing workflows and constrained interpretation. Among the many methods developed include lineament (edge detection)

tracking which has significantly helped and improved rapid structural mapping. Brewster et al. (2014) has reported on such software *Contact Lineament Processing* giving examples from Brazil and the Philippines. A further example from Peru it given by Murphy et al. (2014). An automated depth estimation method developed by Salem et al. (2013) *Adaptive Tilt-Depth* uses four of the five measured Tensors (T_{xx} , T_{yy} , T_{xz} and T_{yz}) to derive depth estimates. Application of this method by Bell Geospace using different source types to provide depth estimates, relative to a common datum, show a remarkable consistency when referenced with known geology (C. Murphy, pers. comm. 2017).

AIRBORNE GRAVITY METER SYSTEMS

Many advances have been made in the design and operation of airborne gravity acquisition systems to allow them to operate on the same flying platform as the magnetic and/or radiometric instruments, making for a highly efficient survey system for natural resource mapping and targeting. Since gravity sensors are relative measuring instruments there is an important operational requirement to accurately tie measurements into airstrip base station values as well as monitoring instrument drift. The accuracy and resolution of the final gravity map has improved by flying slower, having closely spaced flight lines and an instrument that is able to perform in turbulent air conditions allowing loose drape flying. This coupled with improvements in DGPS technology and instrumentation now make it possible to achieve wavelength resolution for gravity of better than one kilometer. Aircraft-independent operations are now routine with fully automated recording. Quality control is now routinely done in-field as is preliminary map production.

Three of the airborne gravity sensor systems available for survey include:

TAGS-6 (Figure 2): The MicroLaCoste TAGS-6 system has evolved from the earlier LaCoste-Romberg highly damped zero-length spring gravity sensor of the mid 1990s via the Marine Air II and TAGS/Air III meters to the present TAGS-6 dynamic gravity meter. Significant improvements have been made to the spring tension tracking loop as well as the stabilized platform

control loop. For repeat lines, such a system with a 100-s filter now has a standard deviation of 0.73 mGal (www.microglacoste.com).

GT-2A (Figure 3): The GT-2A system started commercial operations in late 2008 and was designed by the Russian company Gravimetric Technologies using an accelerometer reference mass in the form of a flat coil located within a gap of a differential magnetic system, consisting of four temperature-compensated magnets. It relies on a Schuler-tuned three-axis inertial stabilized platform with a vertically constrained gravity accelerometer sensing element. The GT-2A system replaced the GT-1A system (launched in 2003) and has significantly improved its performance particularly in turbulent flight conditions and in loose drape flying mode. These improvements included a new shock mount and vibration isolation system to removed vibrations seen in the original GT-1A data and a new vertical gravity sensor which has twice the dynamic range (Olson, 2010). Under typical conditions, the GT-2A system is capable of accuracy values better than 0.5 mGal for 100-s down-line filter length and consistently delivers results of better than 1 mGal at a 100-s full-wavelength down-line filter with an overall average of better than 0.7 mGal. (www.canadianmicrogravity.com; agp@aerogeo.ru).

AIRGrav (Figure 4): Unlike the TAGS-6 and GT-2A systems which are commercial systems available to survey companies, the AIRGrav is a proprietary system developed and operated solely by Sander Geophysics. This system consists of three-axis gyro-stabilized inertial platform with three orthogonal accelerometers. A Schuler-tuned inertial platform is used to maintain the vertical orientation of the gravity meter independent of the aircraft accelerations due to turbulence, aircraft vibrations and drape flying. The instrument is capable of operating in typical flying conditions experienced in aeromagnetic surveys and has been demonstrated to consistently deliver results of better than 0.6 mGal for a 100-s full-wavelength down-line filter (www.sgl.com).

Comparative tests between instruments are not common. However, Studinger et al. (2008) have compared the performance of the AIRGrav and GT-1A for long flight profiles over the Canadian Rocky Mountains near Calgary and both systems produced high-resolution data. Compared to the GT-1A system, the AIRGrav system had a lower noise level and higher accuracy, and is less sensitive to changing flight conditions, in particular to vertical accelerations during turbulent flights.

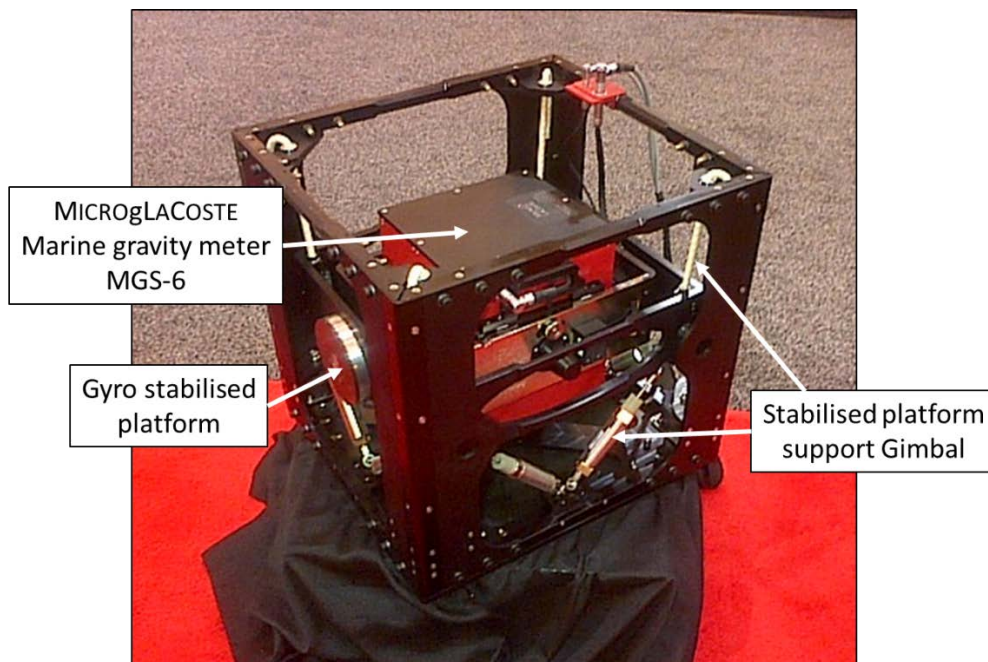


Figure 2: The TAGS-6 gravity system.

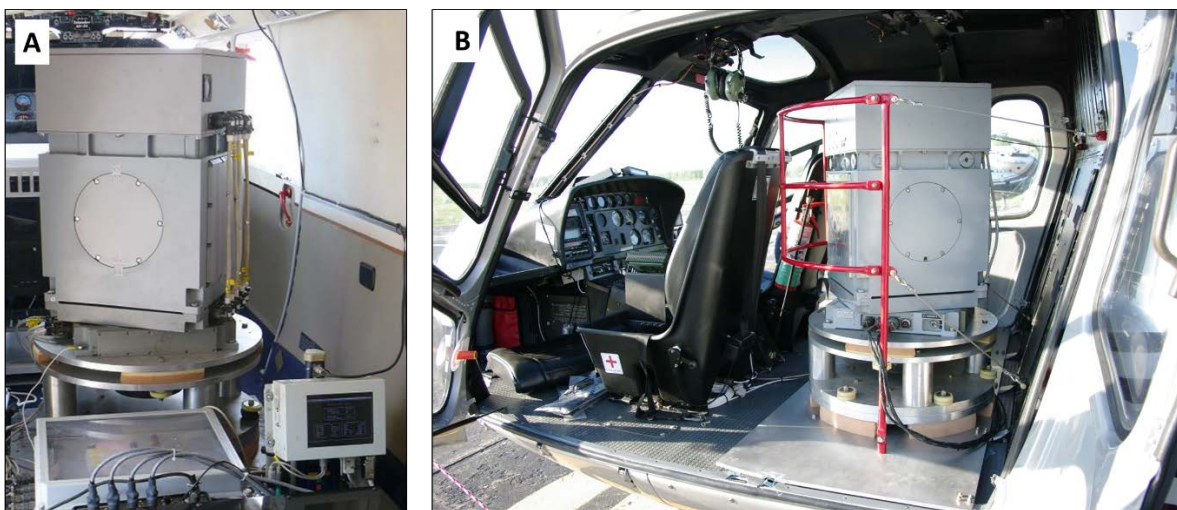


Figure 3: The GT-2A gravity system installed in A: BN-2A Islander aircraft; and B: Helicopter.

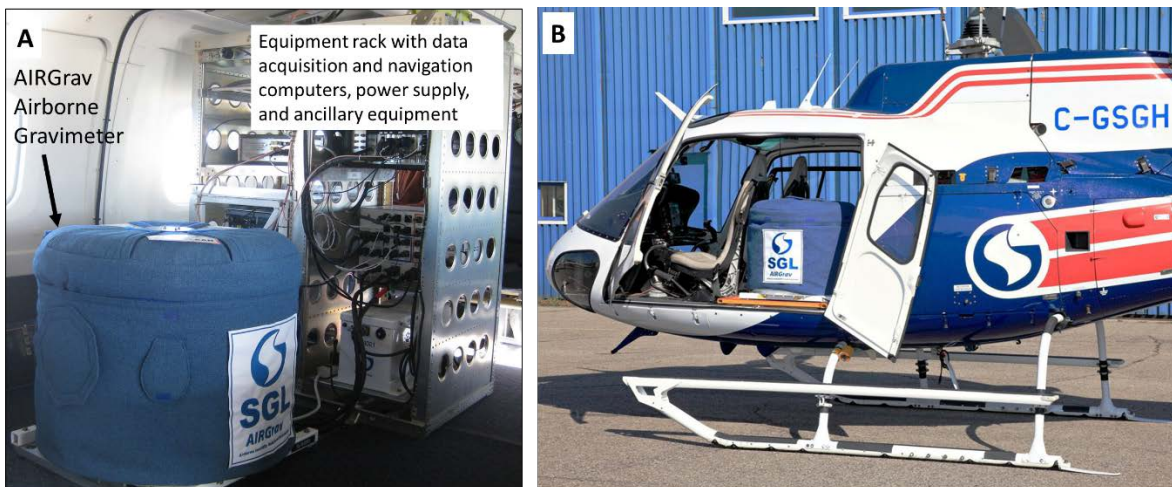


Figure 4: The AIRGrav system installed in A: Cessna Grand Caravan; and B: Helicopter.

GRAVITY SURVEY DESIGN AND PROCESSING

Processing of airborne gravity data involves a sequence of processing steps that include the subtraction of the vertical accelerations of the aircraft that are measured using high quality differentially corrected GPS data from the vertical accelerations measured by the gravity meter, and the application of standard corrections to remove the effects of the rotation of Earth, the movement of the platform over the globe, and terrain effects (Sander et al., 2004). Such processing steps can successfully extract gravity data from very dynamic aircraft environments where accelerations can reach 1 m/s^2 , equivalent to 100,000 mGal. Using high precision differential GPS processing techniques and a robust gravimeter system can result in final processed gravity grids, with noise estimates of 0.1 to 0.3 mGal, having a resolution of 2 km. Although contractor's processing methods tend to be confidential, Sander and Ferguson (2010)

have reported that this standard processing sequence can be enhanced by advanced analysis and improved filtering of the data. These advances involve the use of GPS phase angle corrections, the integration of GPS processing with inertial data from the gravimeter, and the analysis of system states and uncertainties. Such processing has helped to reduce system noise and has allowed the generation of high quality, low noise raw gravity data through a wider range of survey conditions than was previously possible. The processing improvements have been quantitatively assessed by evaluating the average standard deviation for repeat test lines (flown at the start and end of each flight) before and after applying the enhanced processing method i.e. the enhanced method showed a better repeatability for all test lines.

Overall survey resolution can be improved by having closer line spacing and/or incorporating repeated lines because the data are averaged in a manner similar to weighted average stacking of seismic data and closer lines provide more data to average,

which results in less noise; and the terrain corrections are more accurate because the survey system is able to measure the terrain with a higher resolution. The end result of closer line spacing is data with lower noise levels and higher resolution, which can be more accurately modelled and interpreted. (Sander et al., 2003)

Survey resolution can also be improved by flying slower (Wooldridge, 2010; Fairhead 2016). With fixed wing planes there are limitations which are removed when using helicopters. For mineral exploration, a higher resolution dataset is preferable. The AIRGrav systems have been installed in helicopters and in 2009 a number of small survey blocks were flown at an extremely slow acquisition speed (30 knots, equivalent to 56 km/hr or 16 m/s, compared to typical fixed wing aircraft airspeed of 100 to 140 knots, equivalent to 185 to 260 km/hr or 50 to 72 m/s) with tight (50 m) line spacing. Scanning laser elevation data were concurrently acquired in order to create a high resolution 1 m grid cell size digital terrain model. This configuration, coupled with the enhanced processing technique, resulted in a gravity dataset that met the requirements of this mineral exploration project with an accuracy of 0.4 mGal at a 300 m resolution. The accuracy was calculated using the even-odd grid comparison method (Sander et al., 2002) and the results and interpretation of the data from this survey are discussed in detail by Baranyi and Ellis (2010). As Figure 3B indicates the GT-2A system is also operational within a helicopter.

Although airborne gravity surveys are mainly carried out for the oil and mineral industries, airborne gravity data are being used to constrain the water depth of subglacial cavities beneath several floating glaciers and ice shelves off Antarctica (Millan et al., 2017) and has successfully measured with high repeatability the horizontal gravity components (Ferguson et al., 2012).

AIRBORNE MAGNETOMETER SYSTEMS

High resolution airborne scalar magnetic surveys are not new, and over the last decade there has been a steady improvement in absolute measuring magnetic sensor design together with improvements in magnetic compensation (FitzGerald and Perrin, 2015), survey design and GPS controlled navigation allowing more accurate flight path data recovery. These advances, as well as having a magnetically clean aircraft, have all contributed to the progressively higher resolution of airborne magnetometer surveys and as a result have often warranted the resurveying of areas originally flown using instruments and methods that are now considered obsolete.

In recent years the airborne absolute magnetometer system of choice has been the cesium vapour optically pumped magnetometer (www.geometrics.com; www.scintrexltd.com) although recently the potassium alkali vapour (www.gemsys.ca) has been introduced.

Cesium optically pumped magnetometer (Figure 5A): The scalar magnetic value of the earth's magnetic field is measured at an optimal angle between the optical axis of the magnetometer and the direction of the geomagnetic field. Departure from the optimal angle causes a shift in the Larmor frequency with a corresponding error in the scalar magnetic value. A way to minimize this error is by using a split-beam

technique that can be flown in a non-oriented or 'strapdown' configuration. Such a magnetometer has a sensitivity of 5 pT, with sensor noise of less than 20 pT, at a sampling rate of 10 Hz and has the capability to measure ambient magnetic fields in the range of about 15,000 to more than 105,000 nT.

Potassium optically pumped magnetometer (Figures 5B and 6): The potassium optically pumped magnetometer operates on a single, narrow electron spin resonance (ESR) line with relatively high Larmor frequency (7Hz / nT). For potassium, the spin resonance lines do not overlap whereas for cesium they are much broader and overlap resulting in a potassium magnetometer sensor having virtually no dependence on sensor – field orientation and does not require calibration. Potassium's narrow spectral lines, results in an order of magnitude higher sensitivity of 1pT / Hz^{1/2} and sampling interval of 20 Hz.

Triaxial fluxgate magnetometers: Although triaxial fluxgates, e.g. Mag-03MSL (www.bartington.com), are used as sensors within the magnetic compensation system measuring changes in magnetic field associated with the aircraft as it changes pitch, roll or heading, they are also being used for measuring the strength of vector components or total field of the geomagnetic field because of their low weight and cost. Noise levels are down to < 6pT rms/√Hz at 1Hz.

Since all these magnetometer sensors are lightweight they can be installed in appropriate parts of a fixed wing aircraft e.g. ends of the wings and/or rigid tail stinger (Figures 6 and 7) and on unmanned airborne vehicles (UAV, Figure 8). Being able to undertake optimum gravity and magnetic surveys on the same platform has greatly added to the efficiency and cost of data acquisition making such surveys common in oil exploration blocks prior to seismic exploration.

As with airborne gravity, the ultimate resolution of an airborne magnetic survey is controlled by the accuracy of the corrections applied to the sensor data and the survey design. For airborne magnetic data there is a need to make the aircraft as magnetically quiet as possible which involves modifications to clean up the electrical wiring (using twisted pairs and removing ground loops), demagnetizing aircraft hardware and replacing some steel aircraft parts. Corrections to the sensor magnetic data include compensation of the ever changing aircraft's induced magnetic field, diurnal corrections using data from a nearby base station using a similar resolution magnetometer and IGRF corrections based on knowing ones precise DGPS field location within the three dimensionally varying geomagnetic field. All these corrections contribute to the ultimate accuracy of the along flight path survey data.

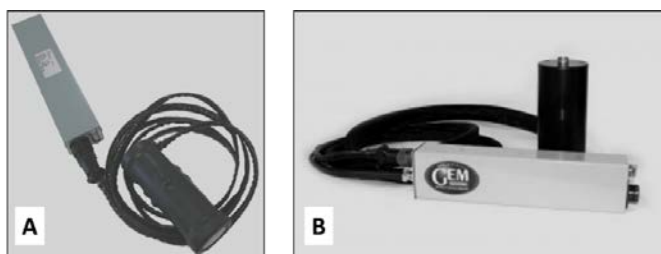


Figure 5: A: Cesium sensor; B: Potassium sensor.



Figure 6: Airborne magnetic configurations for A: Fixed wing aircraft with tail plane having vertical gradiometer stinger; B: Helicopter suspended vertical gradiometer bird. Both systems are using Potassium optical pumped magnetometers.

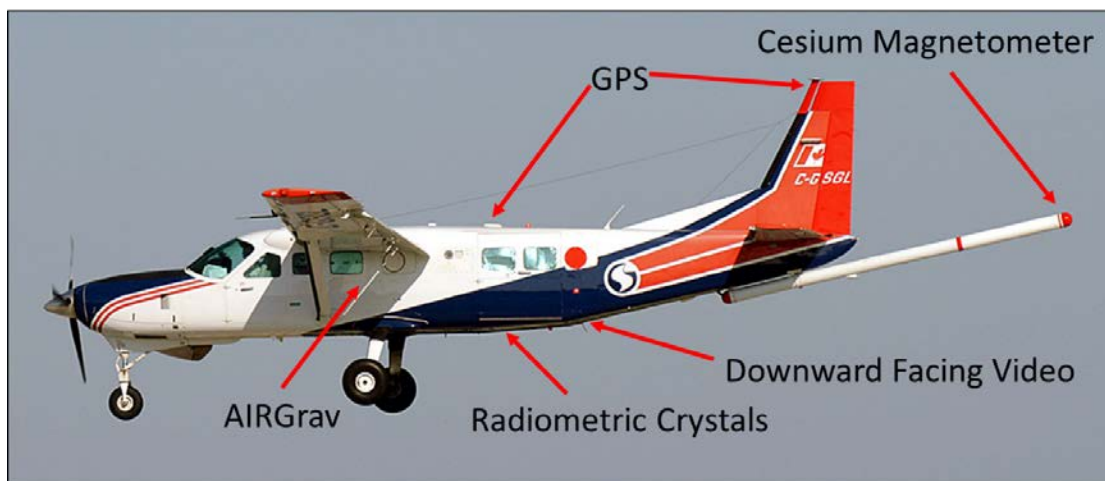


Figure 7: Survey equipment set-up for a Cessna Grand Caravan.

SURVEY DESIGN AND FINAL GRID/MAP CONSTRUCTION

The spatial resolution of the final grid/map is controlled primarily by the flight height and line spacing and overall survey design based on prior knowledge of the geological targets and structures. This is aided by a pre-survey design stage using the known digital terrain model for the study area and designing the survey flight program so that the two orthogonal survey primary and control line directions are flown at optimal flight altitude (draped surface) during the survey while at the same time ensuring that these flight lines intersect at the same altitude. During the survey, the survey flying program is used to control the real-time DGPS auto navigation in three dimensions and the topographic surface is upgraded using the sum effect of the real-time DGPS position of the aircraft and the aircraft's radar or laser altimeter data. This provides important new input for

terrain corrections as well as the morphology of the ground surface that often relates closely to the underlying geology.

The most noticeable short wavelength magnetic features seen in an initial total magnetic intensity (*TMI*) map of a study area often come from near surface 'cultural' or man-made structures. To help identify such structures downward-looking digital video data are routinely collected during the survey and used together with an assembly of digital topographic and utility (gas/oil/pipelines) maps all within a GIS environment. The initial *TMI* grid can also highlight deficiencies in the post-acquisition processing in the form of line levelling noise. The presence of 'cultural' noise and line levelling noise need to be minimized and/or removed before the final grid map is constructed.

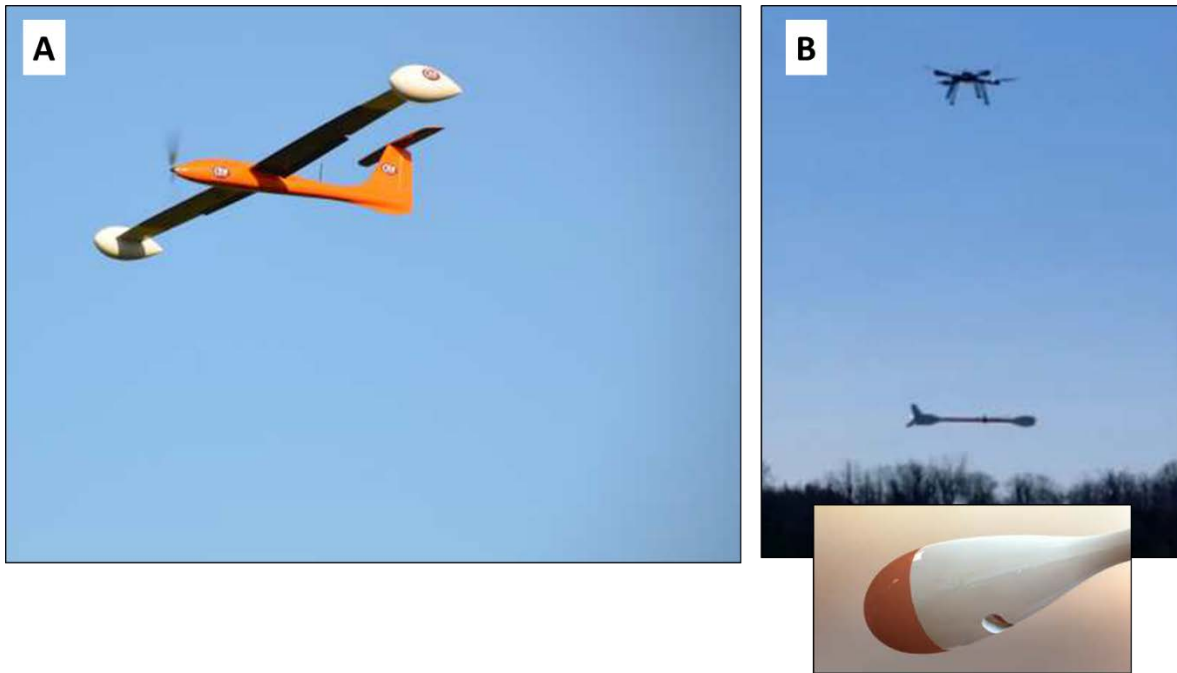


Figure 8: A: An UAV borne magnetic survey drone; B: Lightweight AirBIRD system towing under an UAV with close up view of the instrument pod. Both systems use the potassium magnetometer system complete with power, altimeter, GPS and data radio link.

‘Cultural’ Noise: is a real magnetic signal emanating from often a complex assortment of near surface man-made structures. Manual and semi-automated methods have been developed to help identify and remove such noise from grid based data (Beamish, 2016) and from profile based data (Salem et al. 2010). Both methods use the analytic signal (AS) method. The grid based method employs a moving window correlation method to identify and remove grid nodes associated with the ‘cultural’ anomaly prior to interpolating over the excised data and subsequent regridding. The profile based method is a two stage process. In the first stage, the analytic signal is calculated from the fully processed profile line data and used to identify and remove sections of the profile affected by the cultural noise. In the second stage, the equivalent source approach is used on the remaining parts of the profile to reform the complete ‘culture’ free profile prior to gridding and micro-levelling, if necessary.

Both methods have their limitations particularly in the presence of spatial sets of amalgamated responses and in the presence of near surface geological signals. As such, manual intervention in the semi-automated methods is inevitable.

Line Levelling Noise: results from differences in the fully processed TMI values at primary and control line cross-over points and relate mainly to location errors and inadequate diurnal corrections. Nowadays location errors are very small, due to the accuracy of DGPS positioning systems. However, since diurnal variation of the geomagnetic field varies both spatially and temporally, the diurnal correction can be the main source of cross-over errors. In airborne gravity, inadequacies in the calculation of the: Eötvös correction, drift of the instrument, effects of turbulence and platform stability can all contribute to

line levelling noise and can be minimized by micro line levelling (Fairhead, 2016)

THE ROLE OF LOCAL PHASE & WAVENUMBER IN ADVANCED PROCESSING

Since the early Canadian work by Miller and Singh (1994) it was not until Thurston and Smith (1997) and Verduzco et al., (2004) that the use of the local phase (*Tilt*) and wavenumber derivatives came into common use during the last decade. Such *Tilt* derivatives have the advantage over ‘amplitude’ derivatives of being independent of the susceptibility (and density) of the source structure and thus are able to image more clearly structures at depth. This has led to the development of new methods to delineate structures and estimate their depth. In the latter, the estimate of depth-to-top of magnetic source structures can be seriously biased to a shallower depth if an infinite depth body assumption is used. The *Tilt* can also been applied to downward continuation of data since it is less sensitive to noise than the traditional Fourier domain techniques.

Tilt (or Local Phase or Phase or Phase Angle): When analyzing gravity and magnetic data in terms of geological structures, the total horizontal derivative (*THDR*), vertical derivative (*VDR*), and AS derivatives of the Bouguer gravity and reduced-to-pole (*RTP*) magnetic fields have traditionally been used to map the lateral extent of anomalous density or magnetization bodies and their edges. The derivatives work well, but have limitations in that their amplitude responses are dependent on the density and susceptibility contrasts present. If this contrast is large, the anomaly will also be large whereas if the contrast is small, the anomaly will be small. This is true for

VDR, THDR, and AS derivatives. As such, it may be difficult to image subtle anomalies when in the presence of larger amplitude anomalies. If large amplitude anomalies are present, then the dynamic range of a map will be controlled by these anomalies and the colour fill, using colour equalization, will still preferentially image the larger anomalies. Miller and Singh (1994) were the first authors to refer to the local phase as *Tilt* and in accordance with tradition *Tilt* is used here.

For a profile in the x direction, the $Tilt_x$ is:

$$Tilt_x = \tan^{-1} \left(\frac{\partial T / \partial z}{\partial T / \partial x} \right) \quad \text{or}$$

$$Tilt_x = \tan^{-1}(VDR/HDRx) \quad (1)$$

and contains two ‘amplitude’ derivatives $\partial T / \partial z = VDR$, the vertical derivative or gradient in the z direction and $\partial T / \partial x = HDRx$, the horizontal derivative or gradient in the x direction.

For a grid

$$Tilt_{xy} = \tan^{-1} \left(\frac{\partial T}{\partial z} / \sqrt{\left(\frac{\partial T}{\partial x} \right)^2 + \left(\frac{\partial T}{\partial y} \right)^2} \right) \quad \text{or}$$

$$Tilt_{xy} = \tan^{-1}(VDR/THDR) \quad (2)$$

where $THDR$ is the total horizontal derivative and Figure 9 shows the spatial relationship between these derivative components and *Tilt*.

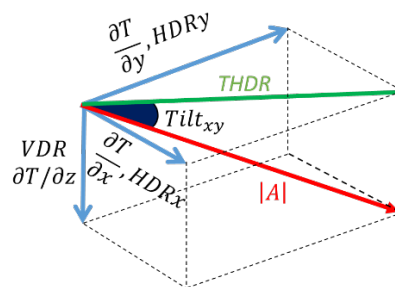


Figure 9: Relationship between the orthogonal derivatives (or gradients) of a magnetic or gravity field and *Tilt*. Normally only the magnitude of the $THDR$ and *Tilt* are measured.

Since within the *Tilt* expression the VDR is divided by the $THDR$ the *Tilt* expression has no dependence on susceptibility (or density) of the underlying bodies. However the *Tilt* does have a dependence on the inclination of the geomagnetic field and this can be eliminated by applying a *RTP*. There are no such problems for gravity data. The arctan function normalizes or limits the *Tilt* value to ± 1.57 radians or $\pm 90^\circ$ and thus provides additional help in visualizing subtle anomalies. An illustration of the enhancement of subtle anomalies is shown in profile form in Figure 10A (after Verduzco et al., 2004) i.e. there is no bias in the amplitude of the *Tilt* anomaly due to magnetic susceptibility variations. Figures 10B-D are also highly informative in grid form, since all positive *Tilt* anomalies relate to positive susceptibility structures which in this case are mainly from dyke like structures with widths that can be estimated from their zero contour crossings. Thus plotting only the positive part of the map helps to simplify the geological complexity of the map (Fairhead et al., 2011; Fairhead, 2016).

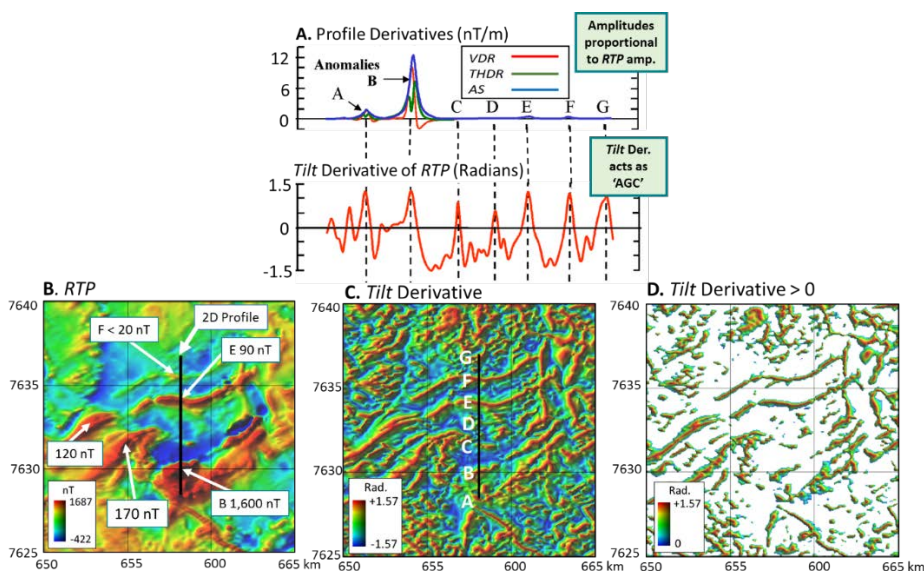


Figure 10: Profile and grid representation of the *Tilt* derivative with respect to traditional derivatives (profile VDR , $THDR$ & AS) and grid RTP for the Erindi gold prospect area, Namibia. The $Tilt > 0$ grid helps to define positive susceptibility structures and their edges.

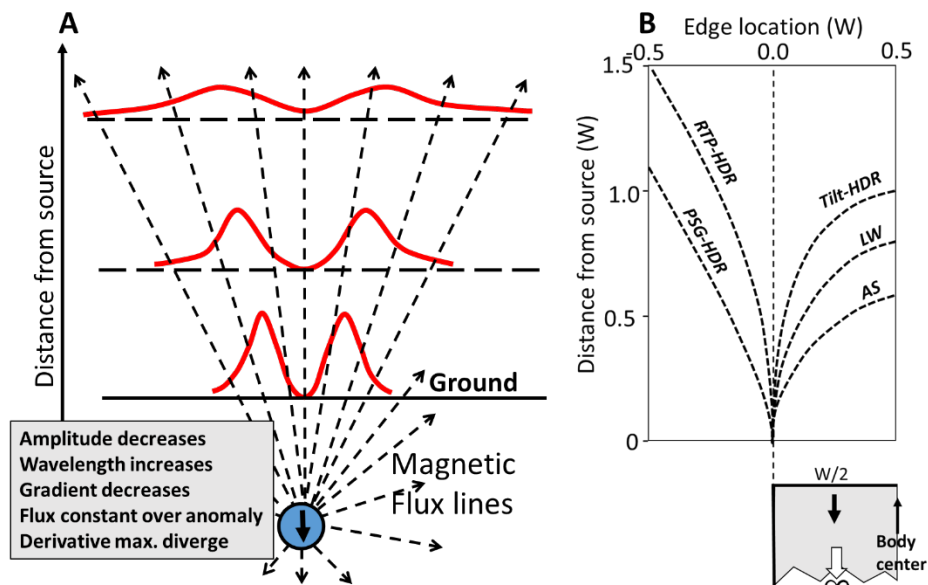


Figure 11: A: Schematic divergence of a magnetic horizontal derivative maximum with distance from the source, B: Quantitative model results of the divergence for a contact model (after M. Pilkington, pers. comm.).

Structural Edges: By careful analysis of gravity and magnetic data it is possible to map edges of structures as well as estimating their depth-to-top (next section). Pilkington (2007) has shown that since gravity and magnetic anomaly fields laterally diverge with increasing distance from the source, then their inflection points and derivative maxima work in the same way (Figure 11B). He showed that the maxima of the horizontal derivative of both the *RTP* and pseudo-gravity (*PSG*) diverging away from the vertical contact, whereas the phase-related derivatives in the form of the horizontal derivative of the *Tilt*, local wavenumber (*LW*) and *AS* diverge in the opposite direction. This property is used by Cascone et al (2012) in an automated grid based process of tracking 2D structural edges by applying a coherency analysis between the maxima of the *THDR* and the zero contour of the *Tilt* (similar to *Tilt-HDR*). Since these two derivatives diverge away from and towards the contact respectively, their mean location is more closely associated with the spatial location of the structural edge. In such analysis it is important to remember that the zero of the *Tilt* is a contour and only part (or parts) of this contour relates to structural edges, whereas the maxima of the *THDR* directly relates to both the length of the structural edge and its susceptibility (or density) contrast. The *Tilt* derivative can also be used to determine the direction of susceptibility and density change across the structural edge (Fairhead et al. 2011).

Finite Tilt-Depth: Depth estimation methods for magnetic sources have long been used to map the depth-to-top of isolated magnetic bodies and basement structures. Many of these traditional methods used infinite depth models (Fairhead, 2016). In 2007, Salem et al (2007) introduced the Tilt-depth method, renamed here the 'infinite-Tilt-depth method' to distinguish it from the 'finite-Tilt-depth method', to estimate the depth-to-top, z_t , for a 2D infinite depth-to-bottom vertical contact model (model A, Figure 12) for *RTP* data:

For an Infinite-Tilt-depth model Salem et al (2007) showed that

$$Tilt = \tan^{-1} \left(\frac{X}{z_t} \right) \quad (3)$$

where X is lateral distance.

When $Tilt = 0^\circ$, then $X = 0$ and is located directly over the contact. When the value of $Tilt = +/-45^\circ$, then the depth-to-top is $z_t = +/-X$, so by measuring the mean distance between the $+/-45^\circ$ contours at any given point along the zero contour, depth z_t can be estimated.

However, although the method is simple, it ignored the fact that the depth-to-bottom of isolated magnetized body will be depth limited. In certain geological settings, such as the USA and other inner continental areas, the depth-to-bottom of the magnetized body, e.g. basement, could be the Curie point isotherm and as such depth estimates to tops of structures within a few kilometres of the surface can be effectively considered to have infinite depth. In other geological settings, such as extended continental margins, the depth to the Curie point isotherm progressively shallows away from the coast whereas the depth-to-top of magnetic basement progressively deepens due to sediment loading and isostasy. In this case, the magnetic based estimates of depth-to-top of basement can be significantly underestimated by several kilometres and may lead to incorrect deductions on the prospectivity of a margin (Salem et al. 2010b; Flanagan and Bain, 2012, 2013) (Figure 12C). Lee, et al. (2010) have further shown that using an infinite depth model for shallow magnetic sources biases and underestimates their depth-to-top. Instead of using 'look up' tables derived by Flanagan and Bain (2012, 2013) to correct the infinite-Tilt-depth estimates to finite depths, Salem et al. (2013) have formulated the finite-Tilt-depth method for *RTP* data. The source geometry

is a vertical sided 2D contact model with lateral extent, X , depth-to-top, z_t and depth-to-bottom, z_b (Figure 12B)

The finite-Tilt- depth model now becomes:

$$Tilt = \tan^{-1} \left[\frac{X(z_b + z_t)}{z_t z_b - X^2} \right] \quad (4)$$

and thus depth-to-top, z_t is

$$z_t = X \left[\frac{z_b + X \tan \theta}{z_b \tan \theta - X} \right] \quad (5)$$

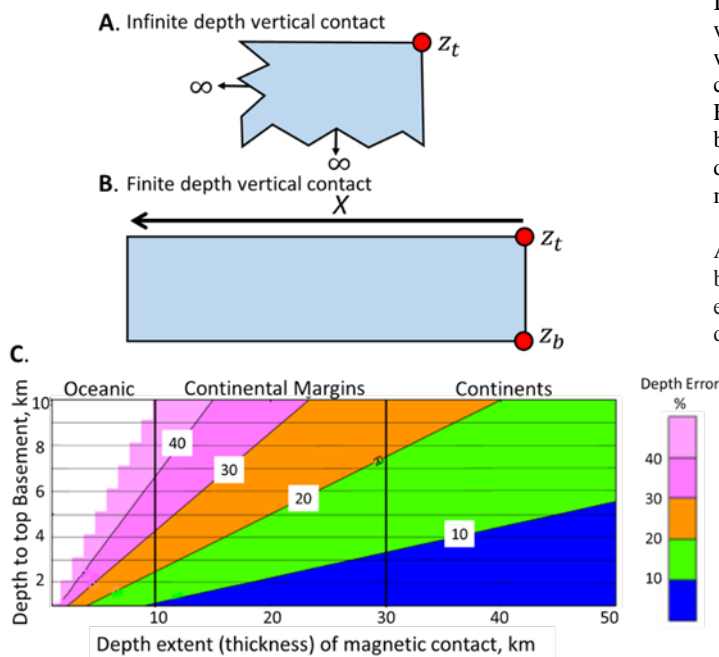


Figure 12: A: The infinite contact model; B: the finite contact model; and C: the error range of z_t resulting from using the infinite depth basement model when the structure has finite depth-to-bottom, z_b .

The difference in depth-to-top using the infinite-Tilt-depth (Salem et al. 2007) and the finite-Tilt-depth (Salem et al. 2013) methods is shown in Figures 12C and 13 for a basement model. After making realistic estimates of X and z_b , the visualization of the results used the zero contour of the $Tilt$ to delineate the edges and the half width between the $\pm 45^\circ$ $Tilt$ contours to colour code the depth. Narrow contours such as $\pm 25^\circ$ can be used (see Salem et al. 2010b). An example of visualization of the finite depth results and differences in depth using magnetic infinite depth results are shown in Figure 13 for the central portion of the Red Sea (Salem et al. 2013). These differences can be very large with the finite depth solutions being up to and greater than a factor of 2 deeper!

A recent application of the Tilt-depth method to calculate depth, location, and dip of thin dykes is given in Cooper (2017).

Downward Continuation: Downward continuation is a process normally applied to magnetic data that reconstructs the data at lower elevations closer to the source. This transformation process is normally carried out in the Fourier domain but has a number of problems due to the presence of high-frequency noise. Great care must be taken in the preparation of the data prior to the application of downward continuation because any Fourier edge effects will be amplified by the downward continuation process. Cooper (2016a) has proposed a simple but novel approach that overcomes many of these problems using the $Tilt$ signal.

In summary, this novel approach rescales the $Tilt$ by a factor α which in effect is equivalent to computing the $Tilt$ from sources with all depths decreased by a factor α . This downward continuation process is much less sensitive to noise than the Fourier transform-based downward continuation processes and because it reduces interference it allows a more accurate source depth determination from methods such as the Tilt-depth method.

As shown in Equation 3, the Tilt-depth can be used to identify both the location of the contact edge ($Tilt = 0^\circ$) and provide an estimate of the depth-to-top, z_t , based on half the physical distance between the $\pm 45^\circ$ contours.

If the depth-to-top of the contact $z_t = 50$ m, then the $Tilt$ will be

$$Tilt = \tan^{-1} \left[\frac{\Delta x_1}{50} \right] \quad (6)$$

and if the depth-to-top of the contact $z_t = 100$ m, then the $Tilt$ will be

$$Tilt = \tan^{-1} \left[\frac{\Delta x_2}{100} \right] \quad (7)$$

The only difference between Equations 6 and 7 is a factor of 2 inside the arctan function. Hence the $Tilt$ from a vertical contact can be transformed into a similar contact at a different depth by the simple application of a scaling factor.

Thus in general, if

$$R = VDR/THDR$$

then

$$Tilt_\alpha = \tan^{-1}[R\alpha]$$

An example of the effectiveness of this downward continuation is shown in Figure 14.

The advantages of the method can be summarized as follows:

- i. By applying factor α of 2, 3, or 4, the resulting $Tilt_\alpha$ moves to within 1/2, 1/3, and 1/4 of the depth to the source depth. The downward continuation of $Tilt_\alpha$ can never exceed the source depth; thus, stability of the $Tilt_\alpha$ grid is preserved.

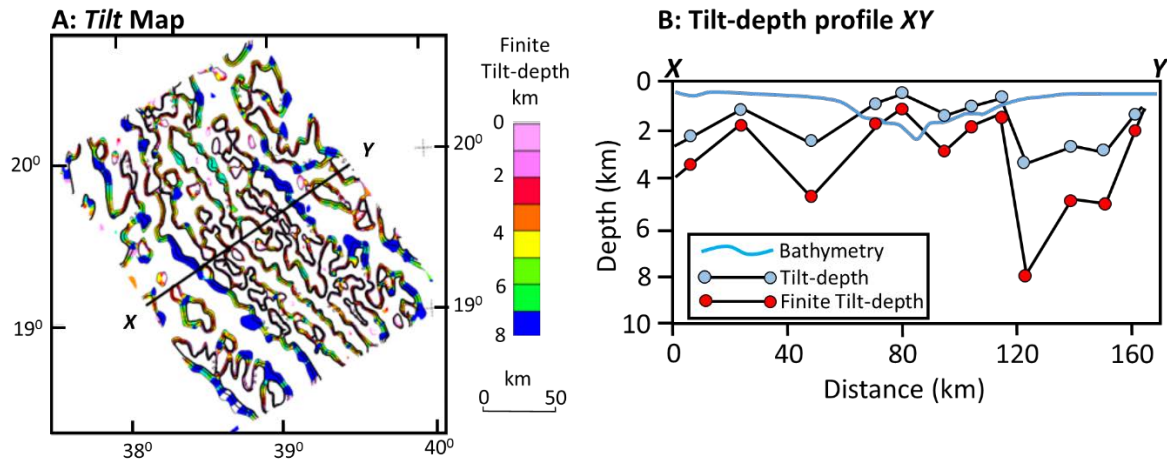


Figure 13: Tilt map of the Central Red Sea with zero contour shown and colour coded contour width $\pm 25^\circ$ used to visualize depth-to-top of magnetic basement. Profile XY shows the difference in depth estimates of z_t for infinite and finite depth models. The depth-to-bottom, z_b , of magnetic basement is assumed to be the Moho derived depth from the seismically controlled gravity inversion.

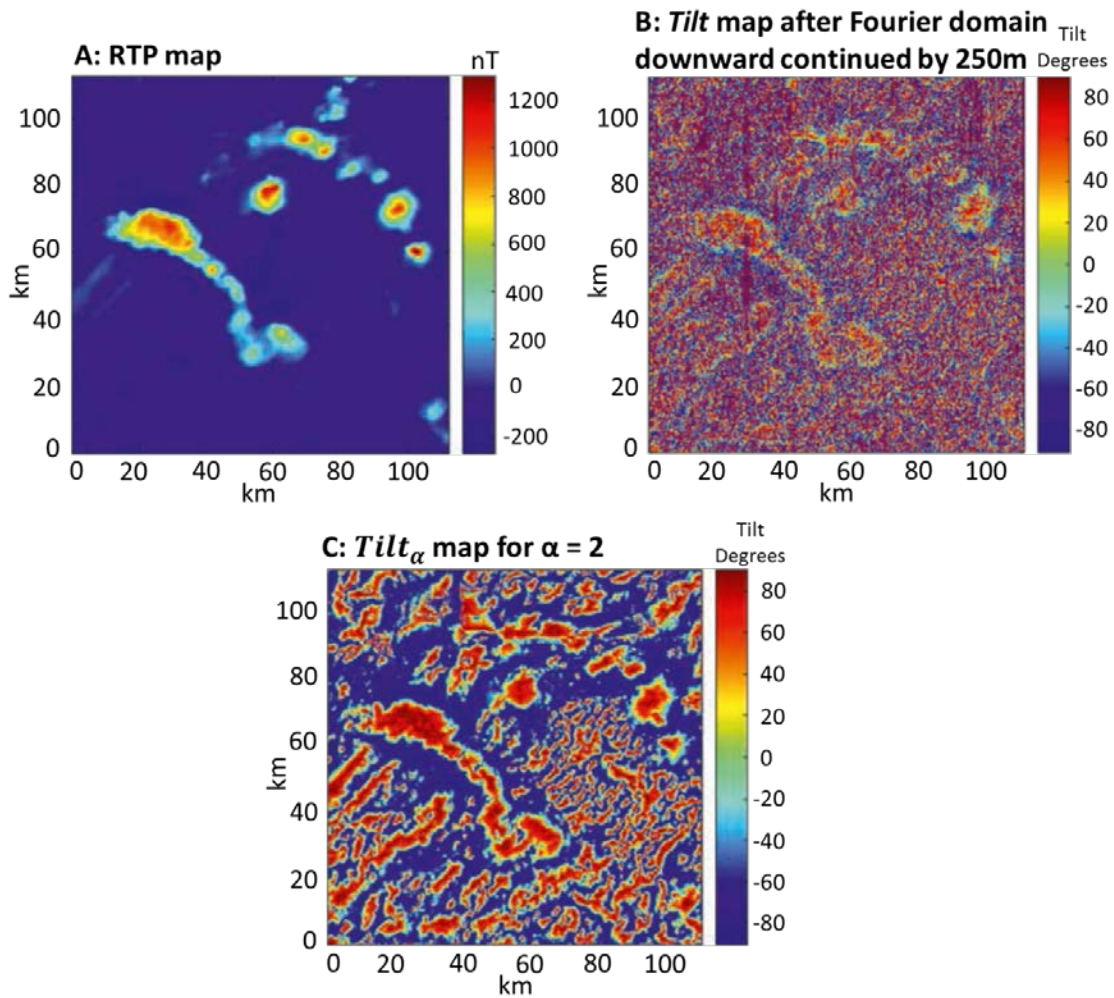


Figure 14: A: Pole-reduced aeromagnetic dataset from Southern Africa with grid spacing 250 m, flight line direction north–south, flight height 100 m and line spacing 1 km; B: Tilt map after downward continuation of the data by 250 m (1 sample interval) using Fourier domain method; C: $Tilt_\alpha$ map for $\alpha = 2$.

- ii. It does not preferentially increase the noise in the signal as traditional downward continuation methods do.
- iii. When factor α is used with the Tilt–depth method, the true depth is $\alpha \times$ Tilt–depth (using h as the half distance between $-45^\circ < |Tilt| < +45^\circ$).
- iv. As indicated in Salem et al. (2010b) and Cooper (2010), h can be measured using other *Tilt* contours, e.g., between $\pm 25^\circ$ such that $z_t = 2.144 h$. This change helps to image maps better and reduce anomaly interference. By applying both the factor α and/or the *Tilt* $\pm 25^\circ$ contour, this reduces anomaly interference and provides better depth estimates.
- v. Application of factor α also acts as an image enhancement method.

When using a factor α , a problem can arise if the sampling interval is insufficient to image the shorter wavelength introduced by applying α . A α value of between 2 and 4 will probably be sufficient for most studies.

Cooper (2016a) has also shown that this downward continuation method can be applied irrespective of the source and magnetisation type if the *Tilt* of the analytic signal amplitude is used.

Local Wavenumber Processing: The *Tilt* is a first order derivative and when used to measure depth-to-top of a structure, it is biased by gradients in the field resulting from the bottom of the structure. When one goes to second order derivatives such a local wavenumber, the rate of change of the field from the top of the structure dominates while that of the structure's shape and bottom diminish. A number of publications relating to depth-to-top using Local wavenumber are Thurston and Smith (1997), Smith et al., (1998) Phillips, (2000), Smith and Salem (2005), Salem et al., (2005), Salem et al., (2010b), Salem et al. (2014) Abbas and Fedi (2015) and Cooper (2017). Cooper (2014) has proposed the 'contact-depth method' which takes the Tilt-depth method to its limits by computing the horizontal derivative of the tangent of the *Tilt* of the magnetic field over the contact. In so doing the method is able to estimate the location, depth, and dip of the contact.

ONGOING DEVELOPMENTS AND FUTURE TRENDS

The last decade has witnessed the spectacular development and exploitation of gravity gradiometer as an exploration tool. Although there is much debate on the final survey noise levels based on AGG and FTG instruments, there is unanimity on such surveys methods delivering exploration results that mining and oil-gas companies need ahead of drilling. The development of instruments and associated systems (software, survey design and application) are not static and the R&D and introduction of newer higher sensitive instruments are likely to have significant impact on exploration over the next decade.

The improvement in the acquisition of airborne gravity data has been one of the significant factors in the last decade such that it is now common practice to jointly conduct gravity and magnetic drape surveys. The limits of resolution of survey data are now

seen more to be the limits on the accuracy of corrections to the data rather than the data themselves. The use of UAV were seen as a major advance but aviation regulations and flight restrictions plus security issues appear to be the limiting factors. Miniaturizing present-day gravity systems for use in UAV is highly unlikely in the near future.

ACKNOWLEDGEMENTS

For the gradiometer section of the paper, the authors wish to thank numerous personnel from CGG, Bell Geospace and Bridgeport for their important technical inputs. On the airborne gravity and aeromagnetic section the authors wish to thank personnel from Bartington Instruments, Canadian Micro Gravity, GEM systems, Geometrics and Scintrex for their technical/instrument/figure input and Mark Pilkington and Ahmed Salem for input to some of the figures.

REFERENCES

- Abbas, M. A. and M. Fedi, 2015, Fractional-order Local Wavenumber – An Improved Source-parameter Estimator: 77th EAGE Conference & Exhibition, Expanded Abstracts.
- Baranyi, E. and R. Ellis, 2010, Gravity Case Study of the Podolsky Deposit, Sudbury Basin, in R. Lane, ed., Airborne Gravity 2010 Workshop, Geoscience Australia Record 2010/21 and GSNSW File 2010/0457, 13-20.
- Barnes, G., 2014, Reconstructing the gravity gradient anomaly field from surveys with wide line spacing using equivalent source processing: an error analysis: Geophysical Prospecting, 62(3), 646-657.
- Barnes, G.J. and J.M. Lumley, 2010, Noise analysis and reduction in full tensor gravity gradiometry data, in R.J. Lane, ed., Airborne Gravity 2010 - Abstracts from the ASEG-PESA Airborne Gravity 2010 Workshop: Geoscience Australia Record 2010/23 and GSNSW File GS2010/0457.
- Beamish, D., 2016, A contribution to aeromagnetic deculturing in populated areas: Geophysical Prospecting, 65(1), 292-304.
- Brewster, J., 2011, Description and evaluation of a full tensor interpolation method: 81st Annual International Meeting, SEG, Expanded Abstracts, 344–347.
- Brewster, J., J. Mataragio and C. Murphy, 2014, A Self Steering Directional Filter For Focused Imaging of Full Tensor Gradiometer Data: 84th Annual International Meeting, SEG Extended Abstracts, 1334-1338.
- Brewster, J., 2016a, Comparison of gravity gradiometer designs using the 3D sensitivity function: 86th Annual International Meeting, SEG, Extended Abstract, 1583-1587.
- Brewster, J., 2016b, Reducing Noise by transforming and combining gravity gradient components: ASEG Extended Abstract 2016.

- Cascone, L., S. Campbell, C. M. Green, A. Salem and J. D. Fairhead, 2012, ACLAS: A new automatic method of defining potential field lineaments using coherency analysis: 82nd Annual International Meeting, SEG, Expanded Abstracts, 1-6.
- Chen, T. and M. Dransfield, 2017, Advances of AGG technologies in CGG, in V. Tschirhart and M.D. Thomas eds., Proceedings of Exploration 17, 16 slides.
- Cooper, G.R.J., 2010, A modified Tilt-depth method for Kimberlite exploration: 72nd EAGE Conference and Exhibition, Extended Abstracts, 4 p.
- Cooper, G.R.J., 2014, The automatic determination of the location, depth and dip of contacts for aeromagnetic data: Geophysics, 79(3), J35-J41.
- Cooper, G.R.J., 2016a, The Amplitude and Phase of the Derivatives of the Magnetic Anomalies of Thin Dykes and Contacts: Exploration Geophysics, 47 (4), 290-295.
- Cooper, G.R.J., 2016b, The downward continuation of the Tilt-angle: Near Surface Geophysics 14(5): 385-390.
- Cooper, G.R.J. 2017, Applying the tilt-depth and contact-depth methods to the magnetic anomalies of thin dykes: Geophysical Prospecting, 65(1), 316-323.
- Dransfield, M., 2007, Airborne gravity gradiometry in the search for mineral deposits, in B. Milkereit ed., Proceedings of Exploration 07, 341-354.
- Dransfield, M. and A. N. Christensen, 2013, Performance of airborne gravity gradiometers: The Leading Edge, 32 (8), 908-922.
- Fairhead, J. D., 2016, Advances in Gravity and Magnetic Processing and Interpretation: EAGE Publications.
- Fairhead, J. D., A. Salem, L. Cascone, M. Hammill, S. Masterton and E. Samson, 2011, New developments of the magnetic Tilt-depth method to improve the structural mapping of sedimentary basins: Geophysical Prospecting, 59, 107-122.
- Ferguson, S. and R. Forsberg, 2012, Geoid Determination from Airborne Vector Gravimetry: American Geophysical Union, Fall Meeting Abstract #G12A-03
- FitzGerald, D. J and J. Perrin, 2015, Magnetic Compensation of Survey Aircraft; a poor man's approach and some re-imagination: Fourteenth International Congress of the Brazilian Geophysical Society, Extended Abstract, 4 p.
- Flanagan, G. and J. E. Bain, 2012, Depth extent: an overlooked parameter in magnetic depth estimation: 74th EAGE Conference & Exhibition, Extended Abstracts, 4 p.
- Flanagan, G., and J. E. Bain, 2013, Improvements in magnetic depth estimation: Application of depth and width extent nomographs to standard depth estimation techniques: First Break, 31, 41-51.
- van Galder, C., 2017, Recent Developments with the Falcon Airborne Gravity Gradiometer, in R.L.L. Lane, ed., Airborne Gravity 2016 - Abstracts from the ASEG-PESA Airborne Gravity 2016 Workshop, in press.
- Hodges, D.G. and Christensen, A.N., 2017, Airborne geophysics, in V. Tschirhart and M.D. Thomas, eds., Proceedings of Exploration 17, 5-16.
- Lane, R. J. L. (editor), 2004, Airborne Gravity 2004 – Abstracts from the ASEG-PESA Airborne Gravity 2004 Workshop: Geoscience Australia Record 2004/18.
- Lane, R. J. L. (editor), 2010, Airborne Gravity 2010 – Abstracts from the ASEG-PESA Airborne Gravity 2010 Workshop: Geoscience Australia Record 2010/23 and GSNSW File GS2010/0457.
- Lane, R. J. L. (editor), 2017, Airborne Gravity 2016 – Abstracts from the ASEG-PESA Airborne Gravity 2016 Workshop: Geoscience Australia, in press.
- Lee, J. B., 2001, FALCON gravity gradiometer technology: Exploration Geophysics, 32, 4, 75-79.
- Lee, M., B. Morris, and H. Ugalde, 2010, Effect of signal amplitude on magnetic depth estimations: The Leading Edge, 29, 672-677.
- Meyer, T., 2017, Recent advances in Lockheed Martin's gravity gradiometer technology, in R.L.L. Lane, ed., Airborne Gravity 2016 - Abstracts from the ASEG-PESA Airborne Gravity 2016 Workshop, in press.
- Millan, R., V. Bernier, M. Morlighem, E. Rignot, and P. Dutrieux, 2017, Researchers find seafloor valleys below West Antarctic glaciers: EurekAlert (eurekalert.org), accessed 18 January 2017.
- Miller, H. G. and V. Singh, 1994, Potential field tilt – A new concept for location of potential field sources: Journal of Applied Geophysics, 32, 213-217.
- Murphy C. A., J. Mataragio, A. J. Olaiz, A. M. Mantilla-Pimiento, G. Zamora-Valcarce and M. García-Gómez, 2014, Exploring the Marañon Basin, Peru, with Full Tensor Gravity Gradiometry technology: 84th Annual International Meeting, SEG, Extended Abstracts.
- Olson, D., 2010, GT-1A and GT-2A airborne gravimeters: Improvements in design, operation, and processing from 2003 to 2010: Airborne Gravity 2010 - Abstracts from the ASEG-PESA Airborne Gravity 2010 Workshop, 152-171.
- Phillips, J. D., 2000, Locating magnetic contacts: a comparison of the horizontal gradient, analytic signal, and local wavenumber methods: 70th Annual International Meeting, SEG, Expanded Abstracts, 4 p.

- Pilkington, M., 2007, Locating geologic contacts with magnitude transforms of magnetic data: *Journal of Applied Geophysics*, 63, 80–89.
- Pilkington M. and P. Shamsipour, 2014, Noise reduction procedures for gravity-gradiometer data: *Geophysics*, 79(5), G69–G78.
- Price, A.D., A. Cacheux, P.R. Chowdhury, G.Shields, J.Weber and R.Yalamanchili, 2013 Airborne gravity gradient acquisition for oil exploration in Uganda: 76th EAGE Conference & Exhibition, Expanded Abstracts.
- Reeves, C. V., S. W. Reford, and P. R. Milligan, 1997, Airborne geophysics: old methods, new images, in G. Gubins, ed., *Proceedings of Exploration 97: Fourth Decennial International Conference on Mineral Exploration*, 13–30.
- Salem, A., D. Ravat, R. Smith, and K. Ushijima, 2005, Interpretation of magnetic data using an enhanced local wavenumber (ELW) method: *Geophysics*, 70, L7–L12.
- Salem, A., S. Williams, J. D. Fairhead, D. Ravat, and R. Smith, 2007, Tilt-depth method: A simple depth estimation method using first-order magnetic derivatives: *The Leading Edge*, 26, 1502-1505.
- Salem, A., S. Williams, E. Samson, J. D. Fairhead, D. Ravat and R. J. Blakely, 2010a, Sedimentary basins reconnaissance using the magnetic tilt–depth method: *Exploration Geophysics*, 41,198–209.
- Salem, A., J. D. Fairhead, and E. Aboud, 2010b, Extended tilt depth – a fast depth imaging method using local wavenumbers of magnetic data: 72nd EAGE Conference & Exhibition, Extended Abstracts, D046.
- Salem, A., S. Campbell, L. Moorhead, and J. D. Fairhead, 2013, An Enhanced Tilt Depth Method for Interpreting Magnetic Data over Vertical Contacts of Finite extent: 75th EAGE Conference & Exhibition, Extended Abstracts.
- Salem, A., S. Masterton, S. Campbell, J. D. Fairhead, J. Dickinson and C. Murphy, 2014, Interpretation of tensor gravity data using an adaptive tilt angle method: *Geophysical Prospecting*, 61(5), 1065-1076.
- Salem, A., R. J. Blakely, C. Green, J. D. Fairhead, and D. Ravat, 2014, Estimation of depth to top of magnetic sources using the local-wavenumber approach in an area of shallow Moho and Curie point depth — *The Red Sea: Interpretation*, 2 (4), SJ1–SJ8.
- Sander, S., S. Ferguson, L. Sander, V. Lavoie, and R. A. Charters, 2002, Measurement of noise in airborne gravity data using even and odd grids: *First Break*, 20, 8, 524-527
- Sander, S., M. Argyle, S. Elieff, S. Ferguson, V. Lavoie, and L. Sander, 2004, The AIRGrav airborne gravity system: SGL Technical Paper www.sgl.com.
- Sander, S., V. Lavoie, J. Peirce, and R. A. Charters, 2003, Advantages of close line spacing in airborne gravimetric surveys: *The Leading Edge*, 22, 2, 136-137.
- Sander, L., M. Bates, and S. Elieff, 2010, High resolution AIRGrav surveys: advances in hydrocarbon exploration, mineral exploration and geodetic applications: 72nd EAGE Conference & Exhibition, Extended Abstracts.
- Sander, L. and S. Ferguson, 2010, Advances in SGL AIRGrav acquisition and processing: ASEG Expanded Abstracts 2010.
- Smith, R. S., J.B. Thurston, T. Dai, and I. N. Macleod, 1998. ISPI – Improved Source imaging method: *Geophysical Prospecting*, 46, 141-151.
- Smith, R. S., and A. Salem, 2005, Imaging depth, structure, and susceptibility from magnetic data: The advanced source-parameter imaging method: *Geophysics*, 70, 4, L31–L38.
- Stadler C., C. Fichler, K. Hokstad, E.A. Myrland, S. Wienecke and B.Fotland, 2014, Improved salt imaging in a basin context by high resolution potential field data: Nordkapp Basin, Barents Sea: *Geophysical Prospecting*, 62, 615–630.
- Studinger, M., R. Bell, and N. Frearson, 2008, Comparison of AIRGrav and GT-1A airborne gravimeters for research applications: *Geophysics*, 73, 6, 151-161
- Thurston, J. B. and R. S. Smith, 1997, Automatic conversion of magnetic data to depth, dip, susceptibility contrast using the SPITM method: *Geophysics*, 62, 807–813.
- Thomson, S., D. Fountain, and T.Watts, 2007, Airborne Geophysics – Evolution and Revolution, in B. Milkereit ed., *Proceedings of Exploration 07: Fifth Decennial International Conference on Mineral Exploration*, 19-37.
- Verduzco, B., J. D. Fairhead, C.M. Green, and C. MacKenzie, 2004, New insights into magnetic derivatives for structural mapping: *The Leading Edge*, 23, 116–119.
- Wooldridge, A., 2010, Review of modern airborne gravity focusing on results from GT-1A surveys: *First Break* 28, 5, 85–92.